SHOCK WAVE IMPINGEMENT ON BOUNDARY AND ENTROPY LAYERS OF A BLUNT PLATE

V. Borovoy, I. Egorov, A. Skuratov
Central Aerohydrodynamic Institute (TsAGI)
1, Zhukovsky st., Zhukovsky, Moscow region, 1401080, Russia

Keywords: *shock wave, boundary layer, interaction, Stanton number, laminar-turbulent transition*

Abstract

Results of experimental and numerical investigations of shock wave/boundary layer and high-entropy layer interaction on a flat plate at laminar and turbulent boundary layer states are presented. Investigations were carried out within the range of Mach number M_∞=5–10.

It is shown that small bluntness of a plate leading edge leads to a considerable heat transfer weakening (up to 50%) in the interaction region. Some gas-dynamic effects were found, which could simplify the solution of the thermal problem of the hypersonic inlet without significant deterioration of its aerodynamic performance. The increase of bluntness is established to lead to the decrease of the heat transfer in the interference region only up to the 'threshold' value. The subsequent bluntness increase does not influence essentially on the heat flux but results in the increase of pressure losses.

Numerical simulation carried out within the framework of Reynolds averaged Navier-Stokes equations with two-parameters q-ω differential turbulence model correctly reflects the shape and dimensions of the separation zone and heat transfer coefficient distribution behind the reattachment line. But the maximal Stanton number in the vicinity of the reattachment line is overestimated significantly.

1 Introduction

Shock wave/boundary layer interaction is one of the most urgent problems of today's aerodynamics. Intense research in this field has been performed for almost 60 years [1, 2]. Some fundamental features of interference flows have been identified. A large volume of quantitative information has been obtained, and the dependence of the maximum pressure and heat-transfer coefficient on the free-stream parameters and shock-wave intensity has been found.

Research of interference flows has been substantially intensified in the last two decades. The main challenge now is the development of the adequate methods of numerical simulations of the interference flows. Various approaches and various turbulence models are used for the turbulent flow calculations. Significant progress has been achieved by using the advanced computational capabilities [3-5].

Nevertheless, the distributions of heat transfer and friction in the developed separation zones formed by the strong shock waves impinging onto the body surface still cannot be calculated with acceptable accuracy. It was recognized that to solve this problem more experimental data are needed.

Almost all activities aimed at studying interference flows deal with the shock-wave interaction with the boundary layer on a flat plate with a sharp leading edge (or a sharp cone). The effect of the small-radius bluntness of the body on the gas flow and heat transfer in the interference zone was ignored. At the same time, the leading edges of the vehicle must have certain bluntness. It is necessary to reduce the heat flux from the gas onto the leading edge and to restrict the maximum temperature. On the other hand, the bluntness radius of the leading

edges has also to be restricted to avoid an increase in drag and losses of total pressure.

The influence of small radius bluntness on the flow behind a flat plate or a cone in the absence of any incident shock waves was studied carefully in the 1950-1960s [6-8]. It was demonstrated that the high-entropy layer (HEL) generated by the bluntness affects significantly the distributions of pressure and heat-transfer coefficients on the plate (or the cone) surface even at a large distance from the leading edge (or the cone tip). Criteria of similarity determining the influence of the small-radius bluntness on the pressure and heat-flux distributions were established.

The influence of the small-radius bluntness on the flow in the interference zone, however, was first studied only recently by the authors of Refs. [9, 10]. Some gas-dynamic effects were found, which could simplify the solution of the thermal problem of the hypersonic inlet without significant deterioration of its aerodynamic performance.

The effects observed were explained on the basis of the high-entropy layer characteristics; the influence of the Mach number on the 'threshold' value of the bluntness and the maximum heat-transfer coefficient in the interference zone were estimated.

In the works performed the undisturbed boundary layer was in the laminar state, and the laminar-turbulent transition occurred only inside the separation zone generated by the incident shock wave. At the same time, the influence of bluntness on interference between the shock wave and the turbulent boundary layer is of the greatest practical interest. The present work is aimed at experimental and numerical investigation of the 2D interference between the shock wave and the turbulent boundary layer at hypersonic speeds. At the same time, some results concerning shock wave/laminar boundary layer interaction are presented.

2 Model. Experimental conditions

Interference between the shock and laminar boundary layer was studied at Mach numbers M_∞ = 6, 8, and 10, total pressure 8–36 bars, and total temperature up to T_t = 775K. The corresponding Reynolds number $Re_{\infty, L}$ was within the range from 0.22×10^6 to 1.32×10^6.

The plate length was L=120 mm, its width was 150 mm, Fig. 1. HEL is generated by means of the changeable forward adapters with cylindrical bluntness radius from r= 0.1 mm up to 10 mm. The plates are equipped with the heat flux sensors 'thin wall' type. They are located along the plate symmetry axis.

In order to reduce the gas overflow from the inclined plate surface to the flat working one, the side fences are used.

Interference between the oblique shock and the turbulent boundary layer is studied at Mach numbers 5, 6 and 8. The model length was L = 320 mm, its width was 150 mm. Maximal total pressure was raised to 90 bars. Thus, the Reynolds number was up to $Re_{\infty, L}=27\times10^6$ at M_∞=5, 20×10^6 at M_∞=6 and 6×10^6 at M_∞=8. Under these conditions, natural laminar-turbulent transition took place at M_∞=5 near the plate leading edge. In order to achieve the uniform transition at Mach numbers 6 and 8, a trip was used. It represents the three lines of cylinders 0.2 mm in height and 1 mm in diameter located near the plate leading edge.

The oblique shock wave generator is placed under the plate using additional sting. This generator looks like a sharp wedge with the angle θ=15^0. Generator length is 200 mm. Distance from the plate leading edge to the shock impinging point is varied by changing the values ΔX (distance between plate and generator leading edges) and ΔY (gap between plate and generator). These values were chosen taking into account the fact that the bow shock wave of the blunted plate should not fall onto the shock generator surface.

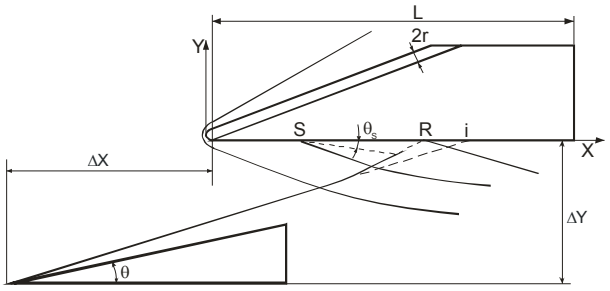

Fig.1. General scheme of the experimental set up

3 Numerical simulation

The Reynolds averaged Navier-Stokes equations with the two-parameter q-ω differential turbulence model [11] were used for the numerical flow simulation. The earlier calculations of the shock-wave/turbulent boundary-layer interaction pointed to the lack of coincidence between the numerical and experimental data in the case of flow over the blunted plates.

In this respect, the parametric calculations were fulfilled using different values of the turbulence constants and free-stream turbulence. Their influence on location and dimensions of the separation zone generated at the interference between the incident shock and the turbulent boundary layer is studied. The following values of the depending variables used in the turbulence model provide a better agreement between the numerical and experimental results: q_∞/V_∞=0.01 and $\omega_\infty L/V_\infty$=0.1. These values characterize the turbulence level and turbulence scale in the undisturbed flow. In the previous work [9], another values were involved in the calculations: q_∞/V_∞=0.003 and $\omega_\infty L/V_\infty$=1. For Mach number M_∞=6 and free-stream temperature T_∞=80 K, the values L=0.1 m and V_∞=1075 m/s are used as the characteristic measures of length and velocity.

4 Results of experimental and numerical investigations

4.1 Laminar flow ahead the shock

The shadow photograph approves boundary layer separation at a sharp plate (Fig. 2). Small separation zone angle (5^0–7^0) is typical for the laminar separation zone. Experimental and numerical distributions of the Stanton number along the plate symmetry line are shown in Fig. 3. Comparison with the numerical calculation confirms the laminar state of the boundary layer right up to the separation line.

The incident shock wave causes the heat transfer intensification. On the sharp plate heat transfer grows more than 30 times. It happens due to the boundary layer separation. In the reattachment region pressure is great and new boundary layer is rather thin. Besides, at flow parameters realized in this work laminar-turbulent transition takes place in the shear layer. Fig. 3 demonstrates that: without taking into account the turbulization, the calculated heat flux values are approximately three times lower than the data with taking into account the turbulization. When the laminar-turbulent transition is taken into account in calculation, data correlates with experimental one.

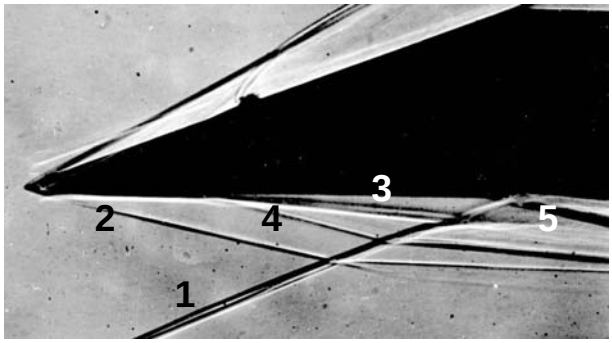

Fig. 2. Shadow flow pattern. Sharp plate. M_∞=6. $Re_{\infty,L}$= 1.3×10^6
1 – incident shock wave, *2* – bow shock wave generated by the boundary layer rising, *3* – boundary of the separation zone, *4* – shock wave generated by the separation zone, *5* – reflected shock wave

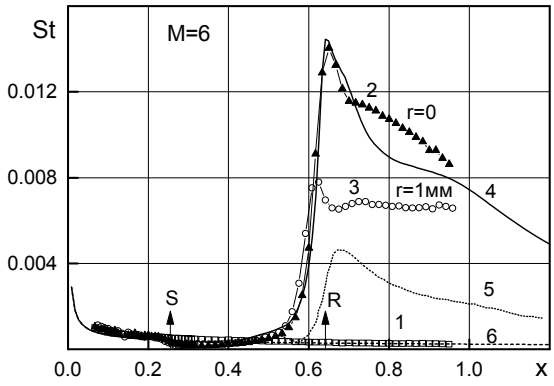

Fig. 3. M_∞=6, $Re_{\infty,L}$ = 1.3×10^6
1, 2, 3 – experiment; *4, 5, 6* – calculations;
1, 6 – r = 0, without shock impinging;
2 – r=0, *3* – r=1 mm, with shock impinging;
4 – r=0, with shock impinging, taking into account the turbulence;
5 – r=0, with shock impinging, without account of the turbulence

Influence of the relative bluntness r/δ^* on the maximum Stanton number St_{mb} is illustrated in Fig. 4. Even a small bluntness results in a

significant weakening of the heat transfer in the interference region. The bluntness effect is especially substantial near the reattachment line where the heat flux is maximal. The effect increases as the bluntness radius grows, but it takes place only up to some 'threshold' value r_{th}. When $r > r_{th}$ an additional increase of the bluntness radius has a small influence on the maximal heat flux. At the increase of Mach number, the bluntness influence on the heat transfer becomes stronger and the 'threshold' bluntness radius becomes smaller.

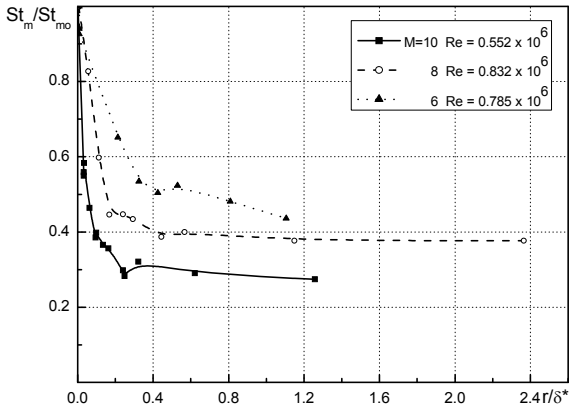

Fig. 4. Influence of the relative bluntness r (δ^*- boundary layer displacement thickness) on the maximum Stanton number St_{mb} (St_{ms} – maximum Stanton number on the sharp plate)

Weakening of the heat transfer due to the leading-edge bluntness and presence of the 'threshold' bluntness are associated with the formation of the high entropy layer with the inherent low gas density. In the presence of HEL, the gas with reduced density due to the admixing from HEL comes in the reattachment line at the end of the separation zone . The bigger is the bluntness, the lower is the gas density in the reattachment region. When the bluntness is big enough, in the reattachment line the gas comes from the HEL only, and the additional increase of the bluntness has a small effect on the heat transfer.

As far as the viscous boundary layer 'swallows' the HEL, the bluntness influence on the heat transfer decreases. The ratio of the bluntness radius to the displacing thickness of the boundary layer can be used as a parameter controlling 'swallowing' of the high entropy layer.

Investigations of the shock wave/laminar boundary layer and HEL interference showed the following:

- Small plate bluntness results in an essential decrease of the heat transfer in the interference region.
- Increase of the bluntness leads to the decrease of the heat transfer in the interference region only up to the 'threshold' value. The subsequent bluntness increase does not influence essentially on the heat flux but results in the increase of pressure losses.
- Bluntness influence on the heat transfer in the interference region enhances as the Mach number increases due to the increase of the total pressure losses in the high entropy layer generated by the bluntness.

4.2 Turbulent flow ahead the shock

Fig. 5 shows shadowgraphs and experimental Stanton number distributions along the sharp plate length at the incident shock location X_i=105 mm. The calculated Stanton number distributions on the sharp plate at the absence of the incident shock in case of the laminar flow (solid line) and turbulent flow (dash line) are shown, too. Results of shadowgraph analysis are presented on the graphs: arrows on the X axis (from left to right) denote the separation point X_s, the incident shock X_i (more exactly, X_i denotes the intersection of the incident shock extension with the plate), the first rarefaction wave coming from the shock generator back edge X_{rw}.

Similar results for the plate with the bluntness radius r=2 mm are presented in Fig. 6.

The following peculiarities can be distinguished in the shadowgraphs: the incident shock wave 1; the bow shock wave 2 generated by the plate bluntness (see, for example, Fig. 6) or a weak shock generated by the boundary layer rising on the sharp plate (Fig. 5); the weak shock wave 3 generated on the sharp plate in the laminar-turbulent transition zone due to the boundary layer thickening (Fig. 5); the shock wave 6 generated by the separation zone

(Fig. 5); the boundary of the separation zone 7; the shock wave 8 formed behind the separation zone as the deflection of the incident shock from the plate; rarefaction waves 9 coming from the back edge of the shock generator.

Outer boundary of the separation zone forms a great angle (16^0-18^0) with the plate surface, that is typical for the turbulent separation flows. The series of the equidistant lines corresponding to the different positions of the separation shock 6 (for example, in Fig. 6) designates fluctuations of the separation zone.

The incident shock wave causes the heat transfer intensification. It starts ahead the separation line, at significant distance from it. At front position of the incident shock (X_i ≈105 mm) and great bluntness radius, the shock influence propagates forward to the leading edge (Fig. 6).

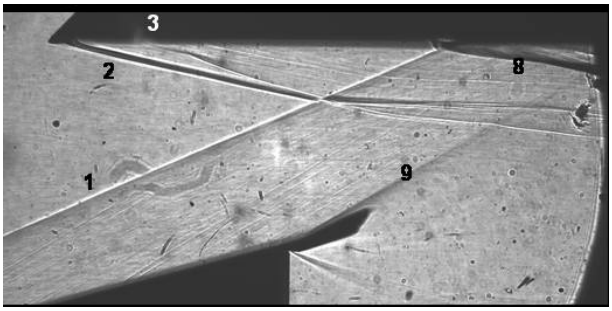

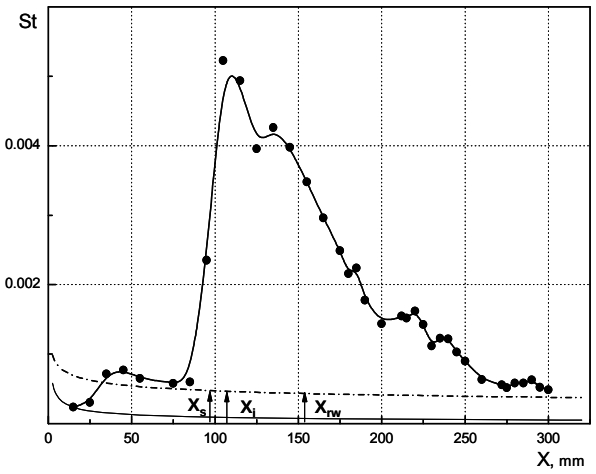

Fig. 5. Shadow flow pattern and Stanton number distribution along the sharp plate surface. M_∞=5, X_i=105 mm

1 – incident shock wave, *2* – bow shock wave generated by the boundary layer rising, *3* – weak shock wave generated on the sharp plate in the laminar-turbulent transition zone due to the boundary layer thickening, *8* – reflected shock wave, *9* – rarefaction waves

Heat transfer coefficient achieves its maximum value behind the incident shock at a small distance from it. The maximal Stanton number St_m in the interference zone is 15.6 times bigger than the calculated Stanton number in the absence of the incident shock at the same line (see the dashed line in Fig. 5 for the turbulent flow on the sharp plate).

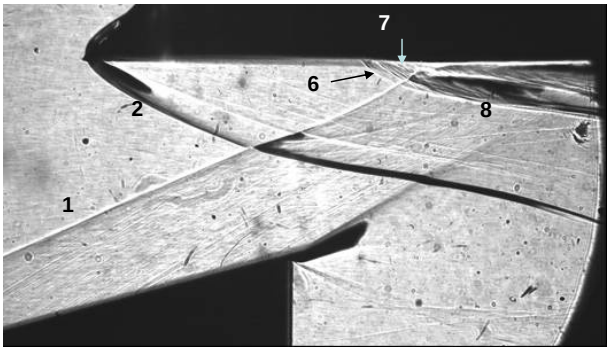

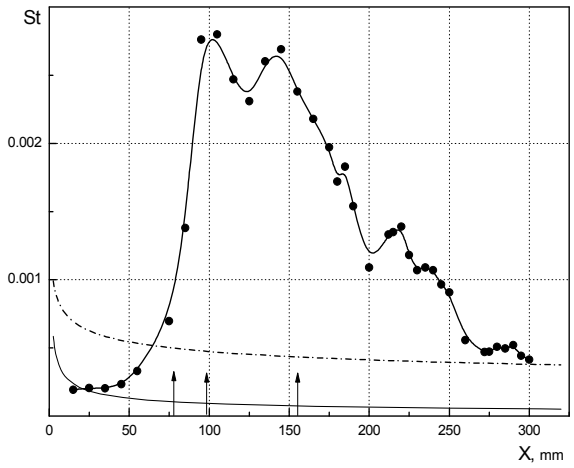

Fig. 6. Shadow flow pattern and Stanton number distribution along the blunt plate surface (r=2 mm). M_∞=5, X_i=105 mm

1 – incident shock wave, *2* – bow shock wave generated by the plate leading edge bluntness, *6* – shock wave generated by the separation zone, *7* – boundary of the separation zone, *8* – reflected shock wave

It should be noted that at M_∞=5 and r=0 in case of inviscid gas flow, the pressure increases approximately 15.6 times across the incident and deflected shocks. In some works, the shock influence on the heat transfer is described by the relation:

$$St_2/St_1 = (P_2/P_1)^{0.8}.$$

According to this relation, at P_2/P_1=15.6 one can obtain St_2/St_1=9.0. The real heat transfer amplification is significantly higher.

Along with the main heat flux peak located near the shock incidence point X_i, the second heat flux peak forms. The reason of such heat transfer non monotony in the interference zone is not found yet. Some hypotheses may be proposed:

- At large total thickness of the high entropy plus boundary layers, the interference zone becomes longer and two types of feat fluxes are generated: one is located near the shock incidence point where the divergence point is formed. The second peak may be associated with the deflected shock formation.
- Near the divergence point arisen at the end of the separation zone, the laminar boundary layer is generated. Then the laminar-turbulent transition takes place resulting in the appearance of the second peak.
- The disturbances coming from the trailing edge of the shock generator cause generation of an additional shock wave.

In Fig. 7 the values l_s and h are shown versus bluntness radius. Here $l_s = X_i - X_s$ is the conditional length of the separation zone, and h is the distance between the plate surface and the intersection line of the separation shock with the incident shock. The values l_s and h vary significantly during the test run due to the oscillations of the separation shock (shadow flow pattern in Fig. 7), and Fig. 7 shows maximal values of h.

Increase of the plate bluntness radius within the range from $r = 0$ to $r \approx 0.5$ mm results in an abrupt expansion of the separation zone. The further increase of the bluntness has a small influence on the separation zone sizes.

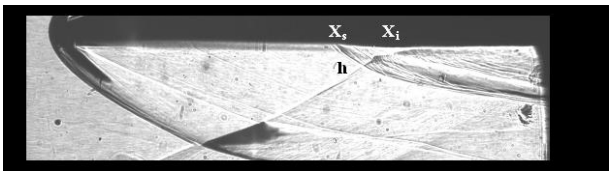

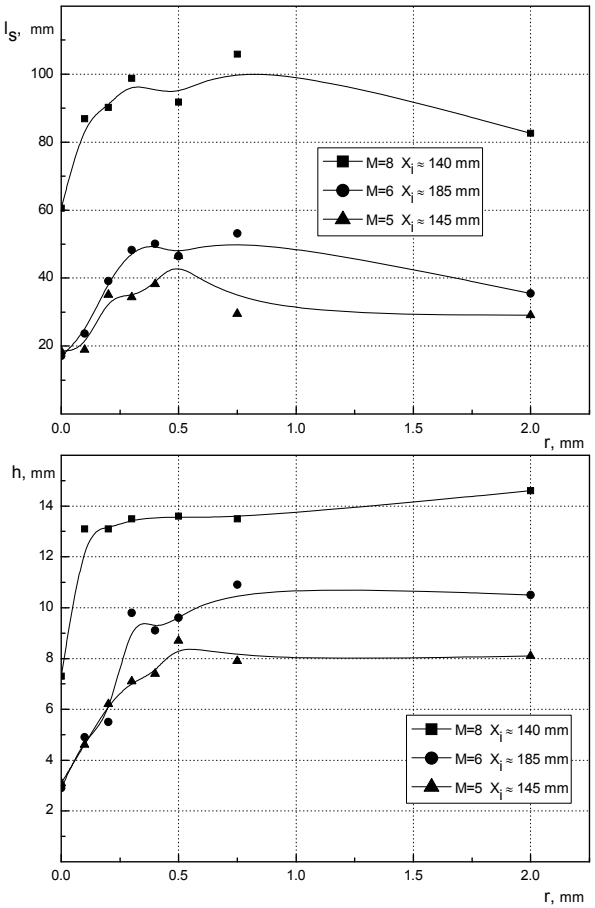

Fig. 7. Separation zone sizes

Fig. 8 illustrates the ratio of Stanton numbers for the blunt and sharp plates versus the plate bluntness radius r at different positions of the incident shock. The values St_{ms} and St_{mb} depend slightly on the shock position. So, the curve 2 presents mainly the dependence of the maximal Stanton number in the interference zone St_{mb} on the bluntness radius. The Stanton number St_m decreases as the bluntness radius increases, but at $r \geq 2$ mm the bluntness radius almost does not influence on St_m. Maximum Stanton number decrease is about 50% of Stanton number value on the sharp plate. Bluntness influence on the Stanton number value outside the interference zone (curve 1 in Fig. 8) is insignificant (within the range of 20%).

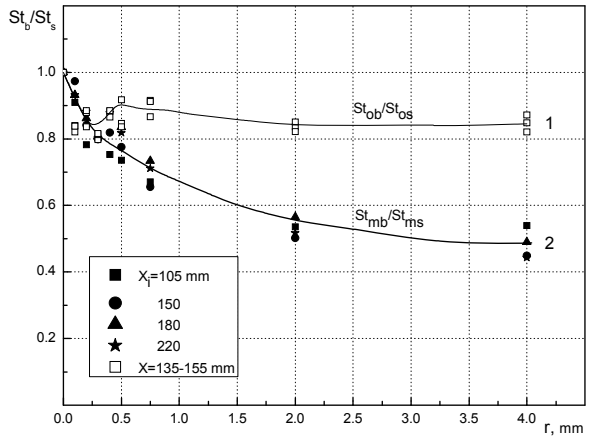

Fig. 8. Ratio St_{mb}/St_{ms} versus the plate bluntness radius. M_∞=5.
1 – without incident shock, *2* – with incident shock. Subscript *s* – sharp plate, subscript *b* – blunt plate, subscript *0* – without interference, *m* – maximal value

Fig. 9 shows the bluntness influence on the maximal Stanton number relative value St_m/St_{m0} at turbulent (solid lines) and laminar undisturbed boundary layers (dashed lines). At the turbulent state of the undisturbed boundary layer, the Stanton number drops slower as the bluntness increases than at the laminar state. Consequently, the stabilization of the heat transfer level in the turbulent case starts at greater radius than in the laminar case. This fact can be considered as a consequence of more intensive 'swallowing' of the high entropy layer by the turbulent boundary layer in comparison with the laminar one.

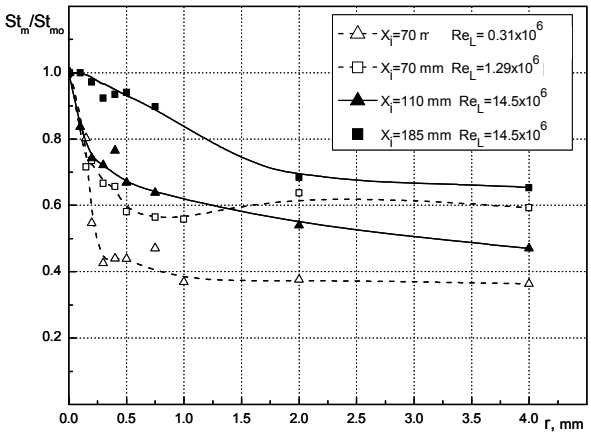

Fig. 9. Leading edge bluntness influence on the maximal Stanton number in the region of the shock incidence on laminar (open symbols) and turbulent (dark symbols) boundary layers at M_∞=6

According to Fig. 9, the maximal weakening of the heat transfer at laminar boundary layer is larger than at the turbulent one.

The calculation and experimental results for sharp and blunted plates (r=0.75 mm) at M_∞=6 are presented in Figs. 10 and 11. In these Figures show the field of $\nabla^2\rho$ values along with the density ρ field. It is done because the photo illumination is approximately proportional to $\nabla^2\rho$ at shadow visualization of the gas flow.

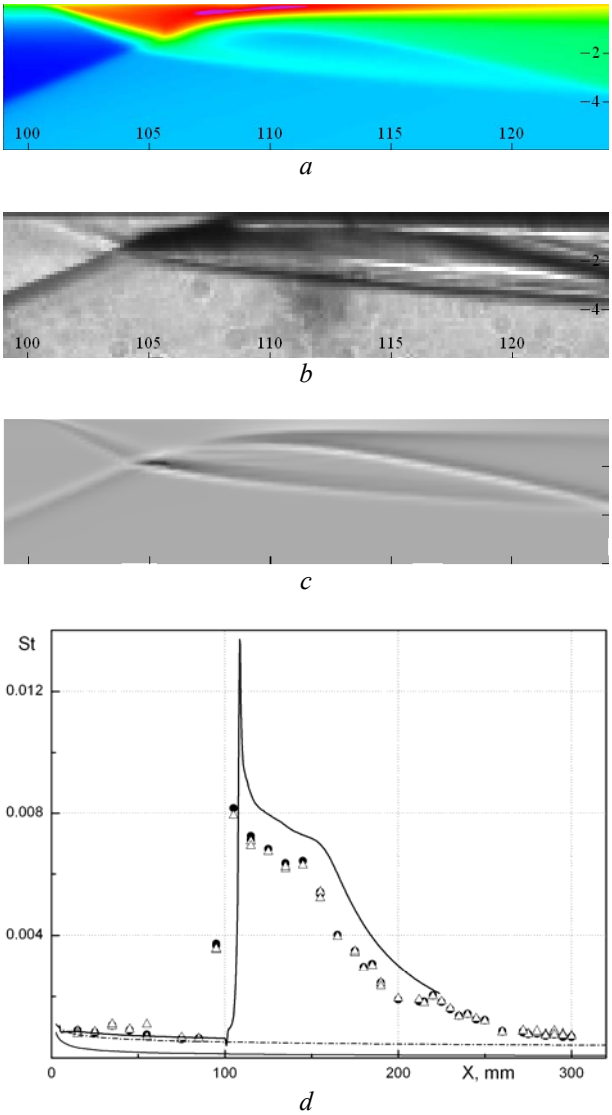

a

b

c

d

Fig. 10. Sharp plate. M_∞=6
a – density field – calculation, *b* – shadow pattern – experiment, *c* – field of $\nabla^2\rho$ value – calculation, *d* – *St* number distribution – experiment and calculation

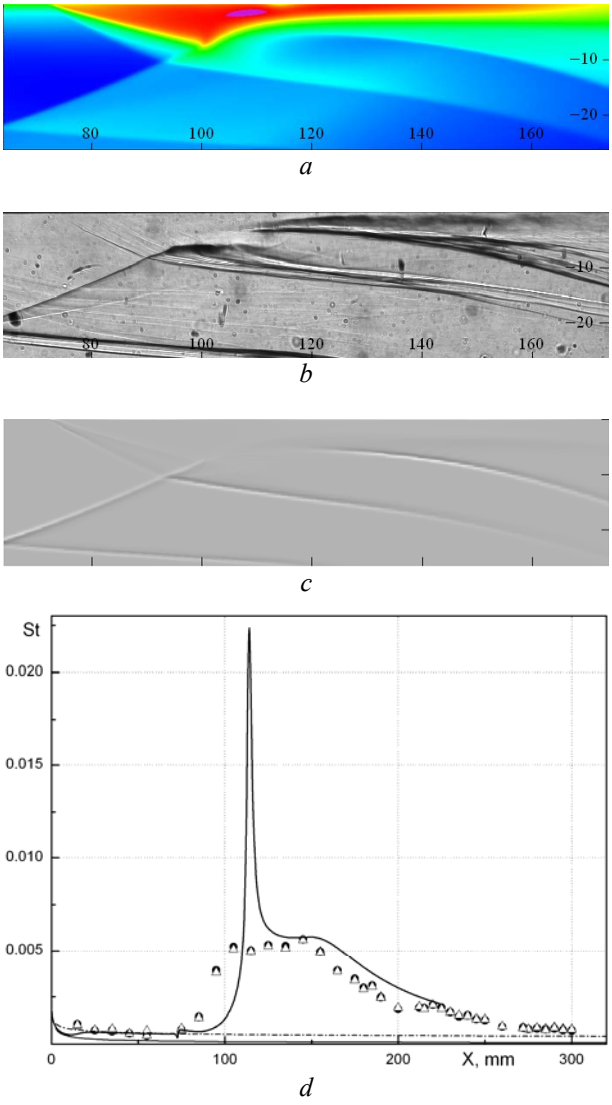

Fig. 11. Blunt plate (r=0.75 mm). M_∞=6
a – density field – calculation, *b* – shadow pattern – experiment, *c* – field of $\nabla^2\rho$ value – calculation, *d* – *St* number distribution – experiment and calculation

At chosen parameters of the turbulence model and free-stream flow turbulence, the calculation results present qualitatively correct description of the location and shape of the separation zone. Over the main part of the interference zone (behind the reattachment line), the Stanton number values are close to the experimental data. According to the calculations as well as according to the experiments, the plate bluntness causes the Stanton number decrease behind the reattachment line. But the calculated peak of Stanton number values in the vicinity of the reattachment line is significantly larger than the experimental ones. The shape of the curve describing the Stanton number distribution in the vicinity of the reattachment line also differs from the experimental shape: according to the calculations, the peak on the blunted plate is sharper than it is observed in the experiments (Fig. 11). Similar conclusion concerning the sharp plate cannot be drawn because of a small length of the separation zone in this case (8 mm only) and scarcity of sensors in the separation zone. The calculation does not reflect the decrease of the maximal Stanton number due to the plate bluntness which is observed in the experiments in all cases. This fact underlines the necessity of further improvement of the method intended for the numerical simulation of the interference between the shock wave, the boundary layer and HEL. From another side, it is necessary to increase the three-dimensional resolution at experimental investigation of the shock-wave/turbulent boundary layer and HEL interaction.

Thus, the investigation of the interference between the oblique shock wave and the turbulent boundary layer and entropy layer of the flat plate at M_∞=5, 6 and 8 shows the following:

- Increase of the bluntness radius results in a significant expansion of the separation zone generated by the impinging shock.
- The impinging shock causes an abrupt increase of the heat transfer on the plate: at M_∞=5 the maximal Stanton number on the sharp plate near the incident shock increases 15.6 times.
- The maximal Stanton number decreases as the plate bluntness increases. But it takes place for the bluntness radius $r \approx 2$ mm only. In this case the Stanton number decreases by 30–50%. Further increase of the bluntness radius has a slight influence on the maximal Stanton number.
- At the turbulent state of the undisturbed boundary layer, the heat transfer weakens, as the bluntness radius increases, slower than in the case of the laminar undisturbed boundary layer.

- The numerical simulation carried out within the framework of Navier-Stokes equations averaged after Reynolds describes correctly the interference flow, including the shape and dimensions of the separation zone and the heat transfer coefficient distribution behind the reattachment point, when the parameters of the turbulent model are properly. But the maximal Stanton number in the vicinity of the reattachment point is overestimated significantly.

This work was supported financially by Russian Foundation for Basic Research (project No. 08-01-00449 and No. 08-08-00565) and ISTC (project #3872), as well as by Federal goal-oriented program "Scientific and scientific-pedagogical personnel of innovative Russia" (state contract No 02.740.11.0154).

References

[1] Delery J. Shock phenomena in high speed aerodynamics: still a source of major concern. *The Aeronautical J.*, pp. 19-34, January 1999.

[2] Dolling D. Fifty Years of Shock-Wave / Boundary-Layer Interaction Research: What Next? *AIAA Journal,* Vol. 39, No. 8, pp. 1517-1531, 2001.

[3] Knight D, Degrez G. Shock wave boundary layer interactions in high Mach number flows–a critical survey of current CFD prediction capabilities. *AGARD AR-319,* Vol. 2, 1998.

[4] Knight D, Yan H, Panaras A, and Zheltovodov A. RTO WG 10: CFD validation for shock wave turbulent boundary layer interactions. *AIAA Paper, 2002-043,* 30 p., 2002.

[5] Zheltovodov A. Advances and problems in modeling of shock wave turbulent boundary layer interactions. *Proc. of XII International Conference on the Methods of Aerophysical Research.* Novosibirsk, 28 June -3 July, Pt. II, pp. 225-236, 2004.

[6] Cherny G. *Gas flows with a large supersonic velocity* (in Russian), Moscow, Physmatlit, 220 p., 1959.

[7] Cheng H, Hall J, Golian T, Hertzberg A. Boundary-Layer Displacement and Leading-Edge Bluntness Effects in High-Temperature Hypersonic Flow. *Journal of the Aerospace Science,* Vol. 28, No. 5, pp. 353-381, 1961.

[8] Hayes W, Probstein R. *Hypersonic flow theory* (in Russian), Moscow, Foreign literature, 607 p., 1962.

[9] Borovoy V, Egorov I, Skuratov A, Struminskaya I. Interaction of an oblique shock wave with the boundary and high-entropy layers on a flat plate. *Izv. Ross. Akad. Nauk, Mekh. Zhidk. i Gaza,* No. 6, pp. 89-108, 2005.

[10] Borovoy V, Skuratov A, Struminskaya I. Existence of a "threshold" value of flat-plate bluntness during interference of an oblique shock wave with the boundary and high-entropy layers. *Izv. Ross. Akad. Nauk, Mekh. Zhidk. i Gaza,* No. 3, pp. 41-52, 2008.

[11] Marvin J, Coakley T. Turbulence Modeling for Hypersonic Flows. *The third joint Europe / US short course in hypersonic.* At the RWTH Aachen – University of Technology, D–5100, Aachen, FRG, 1990.

Copyright Statement